Title

X-ray Absorption Spectroscopic Characterization of the Synthesis Process: Revealing the Interactions in Cetyltrimethylammonium Bromide-Modified Sulfur–Graphene Oxide Nanocomposites

Journal

The Journal of Physical Chemistry C, 120(19)

ISSN

1932-7447

Authors

Ye, Yifan
Kawase, Ayako
Song, Min-Kyu
et al.

Publication Date

2016-05-19

DOI

10.1021/acs.jpcc.6b00751

Peer reviewed

Article

X-ray Absorption Spectroscopic Characterization of the Synthesis Process: Revealing the Interactions in Cetyltrimethylammonium Bromide- Modified Sulfur-Graphene Oxide Nanocomposites

Yifan Ye, Ayako Kawase, Min-Kyu Song, Bingmei Feng, Yi-Sheng Liu, Matthew A. Marcus, Jun Feng, Hai-Tao Fang, Elton J. Cairns, Junfa Zhu, and Jinghua Guo

J. Phys. Chem. C, **Just Accepted Manuscript** • DOI: 10.1021/acs.jpcc.6b00751 • Publication Date (Web): 22 Apr 2016

X-ray Absorption Spectroscopic Characterization of the Synthesis Process: Revealing the Interactions in Cetyltrimethylammonium Bromide- Modified Sulfur-Graphene Oxide Nanocomposites

Yifan Ye[a.b], Ayako Kawase[c.d], Min-Kyu Song[e], Bingmei Feng[b,f], Yi-Sheng Liu[b], Matthew A. Marcus[b], Jun Feng[b], Haitao Fang[f], Elton J. Cairns[c,d*], Junfa Zhu[a*], Jinghua Guo[b,g*]

[a] National Synchrotron Radiation Laboratory and Collaborative Innovation Center of Suzhou Nano Science and Technology, University of Science and Technology of China, Hefei, 230029, P. R. China

[b] Advanced Light Source, Lawrence Berkeley National Laboratory, Berkeley, CA 94720, USA

[c] Energy Storage and Distributed Resources Division, Lawrence Berkeley National Laboratory, Berkeley, CA 94720, USA

[d] Department of Chemical and Biomolecular Engineering, University of California, Berkeley, CA 94720, USA

[e] School of Mechanical and Materials Engineering, Washington State University, Pullman, WA 99164, USA

[f] School of Materials Science and Engineering, Harbin Institute of Technology, Harbin 150001, P. R. China

[g] Department of Chemistry and Biochemistry, University of California, Santa Cruz, CA 95064, USA

ABSTRACT: We have investigated the chemical bonding interaction of S in a CTAB (cetyltrimethylammonium bromide, $CH_3(CH_2)_{15}N^+(CH_3)_3Br^-$)-modified sulfur-graphene oxide (S-GO) nanocomposite used as the cathode material for Li/S cells by S K-edge X-ray absorption spectroscopy (XAS). The results show that the introduction of CTAB to the S-GO nanocomposite and changes in the synthesis recipe including alteration of the S precursor ratios and the sequence of mixing of ingredients lead to the formation of different S species. CTAB modifies the cathode materials through bonding with Na_2S_x in the precursor solution, which is subsequently converted to C-S bonds during the heat treatment at 155°C. Moreover, GO bonds with CTAB and acts as the nucleation center for S precipitation. All these interactions among S, CTAB and GO help to immobilize the sulfur in the cathode, and may be responsible for the enhanced cell cycle life of CTAB-S-GO nanocomposite-based Li/S cells.

1. INTRODUCTION

The increases of global energy consumption and its environmental impact have made sustainable and clean energy technologies highly desirable, especially in the transportation sector. Among the various options, one possibility is to develop suitable electric and hybrid electric vehicles powered by high-performance rechargeable cells that deliver range and power comparable with combustion-engine vehicles. To achieve this goal we need battery cells that are able to provide a specific energy of 350-400 watt-hours/kilogram (Wh/kg) with small capacity decay for 1000-1500 charge-discharge cycles.[1-3] This is beyond the capability of the current best-performing lithium-ion cells in the marketplace.[4] Thus scientists are actively seeking new cell chemistries. One of the potential candidates is the lithium/sulfur (Li/S) cell that could deliver higher power and energy than lithium-ion cells owing to the high theoretical specific capacity of elemental S (1675 mA·h/g). Moreover, the Li/S cell is much more environmentally friendly than the Li-ion cell. These advantages have prompted intense effort to study Li/S cells.[1, 3, 5-9] However, there are technical challenges that preclude the widespread use of the Li/S cell, such as the formation of lithium polysulfides with high solubility in most organic solvent electrolytes. The diffusion of such species during the charge/discharge process leads to the loss of active material, a short cycle life of the sulfur electrode, low utilization of sulfur, and low Coulombic efficiency.[10-11] To address these issues, sulfur is incorporated with conductive carbon materials, such as microporous carbon spheres, porous hollow carbon, porous carbon nanofibers and graphene oxide (GO).[12] This strategy has proved to be effective as these carbon materials with high surface area and porous structure can limit polysulfide dissolution.[1, 7, 13-15] We used GO as a support and conductive agent for the sulfur cathode material, due to its advantages of high carrier mobility, high surface area and excellent chemical stability.[1, 8, 13, 16-17] Thin films of S were deposited onto GO to produce a sulfur-graphene oxide (S-GO) nanocomposite cathode for Li/S cells. It was found that: (a) the GO component is partially reduced by the incorporation of S and thus the conductivity of GO is

improved; (b) the carbon rings and oxygen-containing functional groups (such as hydroxyl, epoxide, carbonyl and carboxyl groups) of GO interact with S, which helps to immobilize S atoms on the GO surface.[18-19] However, these interactions only exist at the inner S layer which is directly attached on the GO surface, limiting the immobilization of S.[3] To further protect the S films, we developed a surface modification method, with the applications of a surface agent CTAB (cetyltrimethylammonium bromide, $CH_3(CH_2)_{15}N^+(CH_3)_3Br^-$).[3] Later, a design of a sandwich structure of CTAB-S-GO was fabricated.[1] With this cathode material and other optimized parameters, the Li/S cells exhibited a very high initial discharge capacity of 1440 mA·h/g of sulfur at 0.2C and excellent rate capability of up to 6C for discharge and 3C for charge while still maintaining high specific capacity (e.g., 800mA·h/g of sulfur at 6C). More remarkably, the cells demonstrated cycling performance up to 1500 cycles with extremely low capacity decay rate of 0.039% per cycle, which is among the best performance reported so far for Li/S cell.[3] This CTAB modified Li/S-GO cell meets most of the requirements for the development of clean engine vehicles with zero emission. Although the cell performance has been significantly improved, an in-depth understanding of the function of the cathode material is still limited. In particular, how S, GO and CTAB interact with each other is still not clear. In the previous study, the interactions between S and GO have been investigated.[19] However the information has been mostly obtained by using C and O K-edge X-ray absorption spectroscopy (XAS) and X-ray emission spectroscopy (XES), which are limited to the observations on the change of the GO. The major element S is rarely mentioned, resulting in a limitation interfering with a complete understanding of the chemical interactions in this cathode material. Moreover, the importance of CTAB in the synthesis has not been realized in the early work and has not been even under discussion in the previous studies. Completely understanding the synthesis procedure helps to optimize the methodology for the controlled synthesis of the desired cathode material that can be used to fabricate a high-performance Li/S cell.

Previously, the XAS technique has established as a powerful tool in the studies of

cathode material structures in various Li-ion cells.[20-24] In this work, we have employed the S K-edge XAS to monitor the evolutions of the S-containing species in each step of the synthesis. S K-edge XAS probes the transition from the S 1s to the 3p orbital. XAS peaks at different photon absorption energies typically represent different S-containing species.[25-26] Combining the XAS spectra profiles with scanning electron microcopy (SEM) morphological investigations and cell performance data, this study elucidates how CTAB is introduced into the cathode material during the sample preparation process, how it further modifies the surface of the S-coated GO, affects the micro structure of the S-GO nanocomposite and subsequently influences the cell performance. Finally, detailed elucidation of the structure-performance relationship for the S-GO nanocomposites is obtained.

2. EXPERIMENTAL SECTION

We followed the process as reported before to synthesize all samples.[3] Briefly, sodium sulfide (Na_2S, anhydrous, Alfa Aesar) and elemental sulfur (99.5% Alfa Asear) were used as the precursors to synthesize the Na_2S_x solution. A GO suspension in the presence of CTAB was added to the Na_2S_x solution during the cathode material preparation process. Finally the mixed suspension was acidified with formic acid, to form the S-GO-CTAB nanocomposite by precipitation. This procedure is illustrated in Figure 1 and described in the Supporting Information. The sample obtained from this procedure is designated as S1-GO/CTAB. By changing fabrication conditions, another two samples were obtained. One (denoted as S2-GO/CTAB) was fabricated by decreasing the amount of Na_2S by 10%. The other one (denoted as S1/CTAB-GO) was fabricated by changing the step in which the CTAB was added, so that CTAB was included in the Na_2S_x solution rather than in the GO suspension. After acidifying the solution, we obtained the precipitated S1/CTAB-GO. After drying at 50 $^{\circ}$C in a vacuum oven for 24 hours, the above three samples were heated in a tube furnace at 155 $^{\circ}$C for 12 hours under flowing Ar with a flow rate of 100 cc/min. The heat treated samples were labeled as S1-GO/CTAB-HT (-HT for heat treated), S2-GO/CTAB-HT

and S1/CTAB-GO-HT, respectively.

To further investigate the reactions in the preparation processes of the CTAB-S-GO nanocomposites, the Na_2S_x solutions were added to the GO suspension and CTAB solution separately. The concentrations of GO suspension and CTAB solution followed the recipe of S1-GO/CTAB. After acidification, the precipitates were collected and named s-S/GO (s- for Solution based chemical Synthesis) and s-S/CTAB, respectively. These two samples after heat treatment were marked as s-S/GO-HT and s-S/CTAB-HT, respectively. Moreover, S and GO (CTAB) powders were physically mixed and studied as well. The physical mixtures of S-GO and S-CTAB before heat treatment were labeled as p-S/GO (p- for Physical mixture of Powder) and p-S/CTAB, respectively. These two samples after heat treatment were marked as p-S/GO-HT and p-S/CTAB-HT, respectively. All the sample information is compiled in Table 1 for easy comparison.

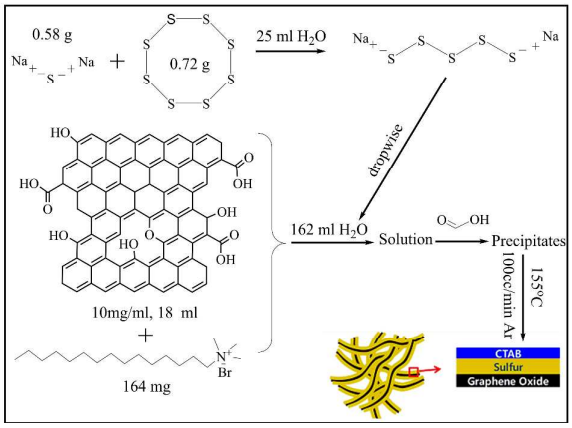

Figure 1: Scheme of sample preparation procedure, recipe of S1-GO/CTAB is taken as an example in the figure.

SEM images were measured using a Zeiss Gemini Ultra-55 instrument. The nanocomposite samples were pressed onto indium foils for the XAS measurements. S K-edge XAS spectra were measured at three beamlines, namely BL5.3.1, BL9.3.1 and BL10.3.2 at the Advanced Light Source, Lawrence Berkeley National Laboratory. The use of the three beamlines is for getting enough beamtimes for a large set of samples, cross-checking the results and verifying repeatability. To eliminate the absorption saturation (also referred to be self-absorption) effect, we used the total electron yield

(TEY) mode. The energy scale for all XAS spectra was calibrated using elemental S spectra assuming the white line to be at 2472.2 eV.

Table 1. Sample designations and XAS peaks

Sample Code	Preparation Process	Peaks	After Heating	Peaks
S1-GO/CTAB	Solution A+CTAB/GO, then + HCOOH	A, B, C	S1-GO/CTAB-HT	A, D, E
S2-GO/CTAB	Solution B+CTAB/GO, then + HCOOH	A, B, C	S2-GO/CTAB-HT	A, D, E
S1/CTAB-GO	Solution A+CTAB, then +GO, then + HCOOH	A, B, C	S1/CTAB-GO-HT	A, D, E
s-S/GO	Solution A +GO, then + HCOOH	A	s-S/GO-HT	A
s-S/CTAB	Solution A +CTAB, then + HCOOH	A, B, C	s-S/CTAB-HT	A, D, E, H
p-S/GO	S powder + GO powder	A	p-S/GO-HT	A
p-S/CTAB	S powder + CTAB powder	A	p-S/CTAB-HT	A, D, E
Solution A: $Na_2S+S \rightarrow Na_2S_x$ Solution B: $Na_2S+S \rightarrow Na_2S_x$, decrease the amount of the Na_2S by 10%				

Table 1: Summary of the sample information including the sample codes, preparation processes and peaks observed (see Figures 3 and 4).

3. RESULTS AND DISCUSSION

3.1. Interactions among the Cathode Materials

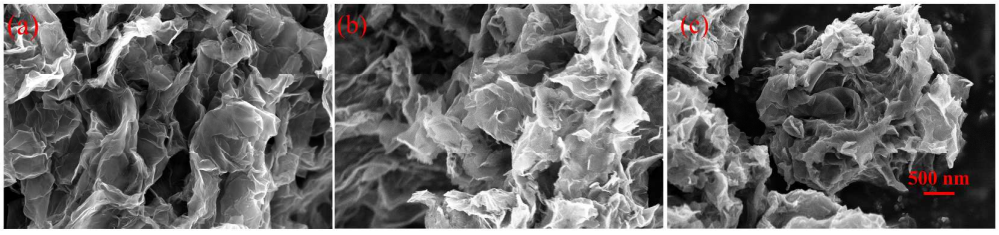

Figure 2: SEM images of samples (a) S1-GO/CTAB-HT, (b) S2-GO/CTAB-HT and (c) S1/CTAB-GO-HT.

During the synthesis of the cathode material, S and Na_2S were used as precursors. The ratio of S:Na_2S is important for determining the sulfur content in the final product. Moreover, the sequence of mixing the GO/CTAB suspension with the sulfur precursor solution is a key point in the synthesis procedure. These changes were investigated by comparing the samples S1-GO/CTAB, S2-GO/CTAB and S1/CTAB-GO.

The layer-like nanostructures with highly developed porous flaky structures of sulfur deposited on GO were reported in the previous reports.[13, 19] Figure 2 shows SEM images of the CTAB-S-GO-HT samples. With the introduction of the CTAB, the unique layered structure was preserved in these samples. In spite of the common layered structures, some morphological differences can be observed. In comparison

with the samples S1-GO/CTAB-HT, S2-GO/CTAB-HT and the previous reports, some agglomeration of GO flakes can be observed in sample S1/CTAB-GO-HT. In addition, visible, though not obvious, agglomeration of GO flakes can also be observed on sample S1-GO/CTAB-HT comparing to the sample S2-GO/CTAB-HT. Therefore it can be concluded that different recipes can influence the morphologies of the cathode materials. Although some slight differences were observed, the basic unique conjugated layer-like structures remain with the introduction of CTAB. These unique structures provide the ability to supply good electrical contact between the electrode constituents, and to accommodate the large volume expansion/shrinkage induced by S and Li_2S conversion during the discharge/charge process. These properties make these CTAB-S-GO nanocomposites promising candidates to make cells that perform well.

In general, morphology difference is always associated with internal chemical structure changes, which cannot be seen directly in SEM images. Therefore, in order to gain chemical information on these samples, we performed XAS experiments. The S K-edge spectra of samples S1-GO/CTAB, S2-GO/CTAB and S1/CTAB-GO are shown in Figure 3(a). We characterized the S species in terms of the positions of peaks in the spectra. Several features can be identified for all the CTAB-S-GO samples: a strong peak appears around 2472.2 eV; and two peaks with lower intensities are observed at 2477.6 eV and 2481.1 eV, respectively. These peaks are labeled as A, B and C, respectively, in Figure 3 (a). Among them, peak A, which is quite close to the S_8 white line, can be assigned to the transition from S 1s core level to the S-S π^* states.[25, 27-28] The strong S-S feature that can be observed for all the CSG samples is attributed to the fact that elemental sulfur is the main product of the reaction between the Na_2S_x and HCOOH solutions. Moreover, in comparison with the spectrum of elemental sulfur,[25] large differences can be observed in Figure 3(a), showing the appearance of peaks B and C. Therefore, it is interesting and unexpected to observe some other sulfur species than elemental S. The appearance of the peaks B and C implies that some new products were formed with the introduction of the CTAB and/or GO during the chemical synthesis process. In addition, the intensities of peaks A, B and C change dramatically under different synthesis conditions, e.g. the

intensity of peak A increases in the sequence of S1/CTAB-GO→S1-GO/CTAB (change of when CTAB is added); and S1-GO/CTAB→S2-GO/CTAB (10% lower Na_2S percentage in the precursors). On the contrary, the intensities of peaks B and C behave oppositely. Therefore we can conclude that the ratio of Na_2S and S in the precursors and the sequence of adding CTAB are directly connected to the new reaction. To identify the origins of the new reaction pathway, it is fairly important to perform detailed studies on these two peaks. Further analysis of the assignments for peaks B and C will be discussed in a later section.

To further analyze the spectra, the white line region is enlarged and displayed in Figure 3 (c). All the spectra were normalized to the white line, and the samples CTAB-S-GO before heat treatment are shown in the bottom of Figure 3(c). Some detailed information can be noted from the enlarged white line region. Firstly, the shoulder of the S-S bond peak, labeled as F, is weaker for sample S1/CTAB-GO compared to that for samples S1-GO/CTAB and S2-GO/CTAB. The previous calculations show that compared with S_8, the six internal atoms of S_8^{2-} do not show shoulder F.[29] Thus, the weaker shoulder F suggests that some of the elemental S may exist in chain, rather than ring form. We can therefore infer that more ring-structure S_8 would be observed on the samples S1-GO/CTAB and S2-GO/CTAB, while for S1/CTAB-GO the sulfur atoms were more likely to be presented as chains. Secondly, a 0.15 eV blue shift of peak A is observed for the S1/CTAB-GO sample with respect to the S1-GO/CTAB and S2-GO/CTAB samples. Considering that the energy difference for the S-S peak position among these samples vanishes after heat treatment, which will be detailed discussed later, we conclude that the peak shift is due to the same cause as the intensity evolution of peaks B and C. We attribute this to the charge transfer from S atoms to the GO and/or CTAB based functional groups. The charge transfer between these functional groups and S may not be strong enough to change the valence states of S (from a spectroscopic point of view), instead, it can cause the blue shift of the peak A.

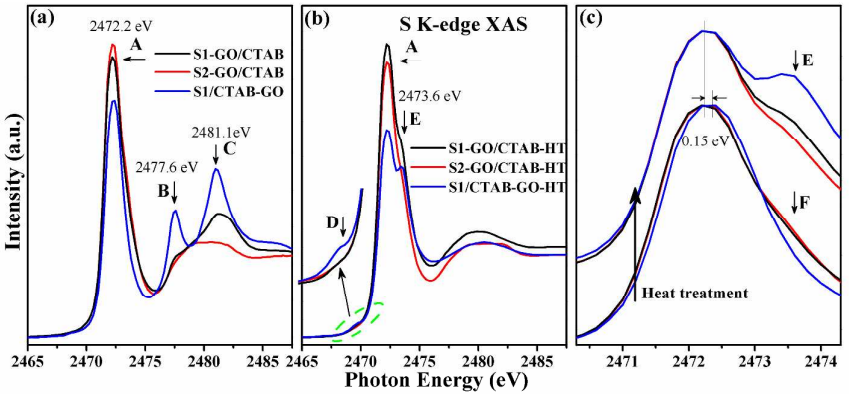

Figure 3: S K-edge XAS data of samples S1-GO/CTAB, S2-GO/CTAB and S1/CTAB-GO (a) before and (b) after heat treatment. The pre-edge region of (b) was enlarged and shown, the white line regions of the (a) and (b) were normalized the peak maximum and shown in (c).

In addition, heat treatment is a critical step, and also the last step, used during the active material fabrication procedure.[1] The heat treatment process helps anchor S to the GO matrix by assisting the diffusion of molten sulfur into the nano-pores of GO.[1, 13, 15] This step could improve the uniformity of the sulfur coating and increase sulfur utilization. To investigate the effect of heat treatment on the chemical interactions, S K-edge XAS spectra of the post-heating samples have been recorded (Figure 3(b)). The pre-edge region is enlarged for better clarity, as shown in the insert. In comparison with the spectra in Figure 3(a), significant changes can be observed in the CTAB-S-GO-HT samples, implying the occurrence of some reactions during the heat treatment. A newly formed peak, labeled as peak E, centered at 2473.6 eV is evident. Peak E represents the transition from S 1s to the C-S σ* state.[18, 25] The appearance of this peak confirms the existence of bonding between S and CTAB and/or GO. Moreover, a small shoulder, labeled as peak D, located at 2470.0 eV is also visible in the spectra. The origin of peak D is still under discussion,[18] and it may be due to the hybridization of S orbitals with CTAB/GO orbitals. Meanwhile, accompanying the appearance of peaks D and E, the peaks B and C vanish during the heat treatment process. Therefore, we can get some information about the species corresponding to the peaks B and C. Firstly, the species appear due to the introduction of CTAB and/or GO; secondly, the species are not stable as they vanish when heated to 155 °C, suggesting they are not associated with the S-O bonding.

Moreover, from the enlarged spectra in Figure 3(c), some detailed information can be noted as follows. Firstly, the peak shift of the white-line is not observed. This is due to the fact that the aforementioned charge transfer effect vanishes when the samples have been heat treated, where the mild interaction is converted to strong C-S chemical bonding. Secondly, the spectrum of sample S1/CTAB-GO-HT shows the strongest C-S bond peak intensity, while that of the sample S2-GO/CTAB-HT shows the weakest. Taking into consideration the spectra before heat treatment, we can conclude that the intensity of each peak, including peak A, peaks B and C and peaks D and E, from different samples change in the order S1/CTAB-GO to S1-GO/CTAB and to S2-GO/CTAB. This indicates the possibility of controllable optimization of the cathode material.

3.2. Roles of CTAB and GO in the Synthesis

To provide further insight into the interactions among the cathode materials, the interactions between S and GO, and S and CTAB have been studied separately. Figure 4(a) displays the S K-edge XAS of physical mixtures of S-GO and S-CTAB. Different spectral evolutions have been obtained for these mixtures. For the S-GO mixtures, the identical elemental S spectra profiles are observed on samples p-S/GO and p-S/GO-HT, which implies that no chemical reaction takes place between S and GO when they are heated at 155 $^{\circ}$C. Similarly, only elemental S peaks are observed for the sample p-S/CTAB, which implies the non-existence of interactions between elemental S and CTAB at room temperature. In contrast, the spectrum of the S-CTAB sample is more complicated after heat treatment, as can be seen from the changes of the spectral shapes. Specifically, the appearance of the peaks D and E accompanied by the decrease of the intensity of peak A has been observed after heat treatment, implying that S can react with CTAB and form C-S bonds at 155 $^{\circ}$C. This process was promoted by the decomposition of the CTAB, as confirmed by the C K-edge XAS and IR shown in Figure S7 and S8, respectively. According to the literature,[30] the decomposition of CTAB occurred upon heating to 155^{o}C, leading to the formation of several products including cetene ($C_{16}^{=}$), cetyldimethylamine ($C_{16}(CH_3)_2N$)) and trimethylamine ($(CH_3)_3N$). S can react easily with C in these species to form C-S bonds. However, to

fully understand the nature of the C-S bonds, further studies are need, which is beyond the scope of this paper. The spectra of the synthesized samples are shown in Figure 4(b). It is interesting to observe that the spectra of s-S/GO and s-S/GO-HT showed typical elemental S spectral profiles, which are similar with what we obtained on the samples p-S/GO and p-S/GO-HT. Therefore, it can be inferred that GO does

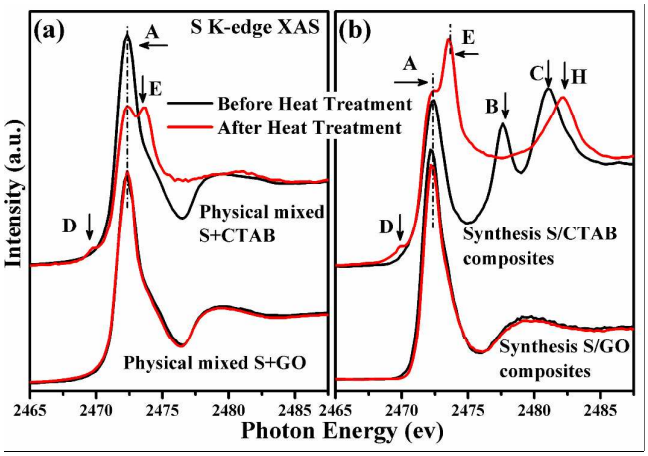

Figure 4: The S K-edge XAS spectra of (a) physically mixed and (b) synthesized S and GO/CTAB before and after heat treatment

not react strongly with either S or Na_2S_x. However, according to the previous studies,[19] the existence of interactions between GO and S were confirmed by the changes of C and O K-edge spectra profiles, including XAS and XES. Therefore, it implies that the interactions of S and GO happened mostly at the interface between GO and S, and this kind of interaction protects the S inner layer well. And also the interactions between GO and S is more likely to be physical adsorption, that is, S can be anchored on the surface of the GO, but this kind of interaction will not be effective in protecting the outer layer of the S films.[3] The absence of the peaks at higher photon energies establishes the fact that the introduction of GO is not associated with the aforementioned new reaction pathway. Therefore, the role of CTAB should be noted and is more complicated than that of GO. This has been further confirmed by the sulfur species evolution observed from the spectra. In Figure 4(b), several peaks can be observed for the sample s-S/CTAB, at the same positions as peaks A, B and C in CTAB-S-GO samples. As discussed above, the peaks A and B/C represent the S-S bond and newly formed species, respectively. The appearance of these peaks

establishes that the origin of the new species is associated with the introduction of CTAB. Moreover, the conversion from sample s-S/CTAB to s-S/CTAB-HT is quite similar with what we recorded on the evolution from samples CTAB-S-GO to CTAB-S-GO-HT, which is presented as the vanishing of peaks B and C and appearance of D and E. Compared with the spectra recorded in Figure 3(b), the intensity ratio of peaks D and E with respect to the S-S peak increased significantly. This can be explained by our previous conclusion, that is: for samples before heat treatment, the stronger the intensities of new-species peaks, the stronger will the C-S bond be formed after heat treatment. As we learn for the peaks B and C, they are associated with interactions of S species and CTAB, meaning that CTAB has been bonded in the materials when the peaks are observed. So the stronger peaks B and C represent a greater amount of S-bonded CTAB or CTAB derivatives. Thereafter, more CTAB can react with S at 155°C and form peaks D and E. Peak H, located at 2482.5 eV, originates from S-O bonds in the SO_4^{2-} specie.[21, 28] The appearance of this specie may be due to the conversion of the remaining S_x^{2-} anions to S^{2-}+S in the solid phase, followed by further oxidation of S^{2-} to stable sulfate. The reason we did not observe the peaks representing the S^{2-} species in the sample s-S/CTAB may be because S^{2-} ions are buried in the sub-surface and protected by S and/or CTAB, leading to the suppression of S^{2-} signal by other S films. After heat treatment, the buried surface is exposed and sulfate species is formed.

Although the exact assignments of the newly formed species evident as 2477.6 and 2481.1 eV peaks in the spectra have not been made, our studies suggest that these species come from the interactions between S species and CTAB, and they are very easy to decompose at 155°C, which is a relatively mild temperature, and form C-S bonds. One interesting observation that should be noted is that some fine particles formed when adding Na_2S_x solution to CTAB solution during the synthesis process of the samples S1/CTAB-GO and s-S/CTAB. The particles were filtered, washed and measured in the usual procedure. The S K-edge XAS spectrum of this intermediate S/CTAB sample shows almost the same spectral shape as that of samples CTAB-S-GO and s-S/CTAB, which show a peak of the S-S bond and two peaks from

the newly formed species (see Figure S1). This observation is further evidence that the formation of the new species that appeared at the higher photon energies starts from the interactions between Na_2S_x and CTAB. To rule out the effect of HCOOH, a control experiment has also been performed: elemental S and CTAB were suspended in the HCOOH solution. The mixture was stirred for 16 hours before the solid particles were collected, washed and measured. The S K-edge XAS spectra of the sample before and after heat treatment show similar spectra shapes with a single peak centering at around 2472.2 eV and a shoulder locating at around 2473.6 eV, which is a typical elemental S_8 spectrum (see Figure S2). Therefore, we can conclude that the CTAB precipitates from solution by interacting with Na_2S_x, or more specifically, CTA^+ interacts with S_x^{2-}. Hence we get explanation for the S K-edge XAS peak intensities change caused by Na_2S:S ratio difference. For the reaction between Na_2S and S, we can write the reaction equation as: $a{\cdot}Na_2S_x = a{\cdot}Na_2S+S$ ($x=1+1/a$). Therefore with the decrease of Na_2S amount (that is "a") in the precursors, the Na_2S_x chain length increases; however, the amount, "a", of S_x^{2-} anions that can bond with CTA^+ decreases. Hence, the remaining CTAB amount in the cathode decreases, causing a decrease of the intensities of peaks B and C. This is consistent with the differences between S1-GO/CTAB and S2-GO/CTAB, which have been shown in Figure 3 (a).

Furthermore, it is also interesting to compare the spectra of samples S1-GO/CTAB, S1/CTAB-GO and s-S/CTAB to evaluate the effect of GO. Firstly, in comparison with s-S/CTAB, S1/CTAB-GO shows a much stronger peak A, while the peaks B and C are not much influenced (see Figure S3). Considering S1/CTAB-GO can be regarded as GO suspension added to sample s-S/CTAB, the spectral changes indicate that GO can act as a nucleation center to enhance the precipitation of S from the solution to solid phase by anchoring S on GO flakes. Therefore, this 2D growth model of the S films enables the uniform deposition of S on the GO flakes. Similarly, when mixing Na_2S_x solution with CTAB first, the S-CTAB precipitates are formed and they can also act as nucleation centers. However, this gives rise to the 3D growth model of the S films and may induce the agglomeration of the nanocomposites. Therefore, the adding sequence

of GO and CTAB during the sample synthesis determines the morphological structures of the cathode. When mixing Na_2S_x solution with CTAB in the presence of GO, a uniform morphology can be obtained, such as that of S1-GO/CTAB and S2-GO/CTAB as shown in Figure 2 (a) and (b). While when mixing Na_2S_x solution with CTAB first, the agglomeration of nanocomposites can be observed, such as that of S1/CTAB-GO, as shown in Figure 2 (c). Secondly, it can be clearly shown that peak intensities of the new species are also influenced by GO, showing as the strong new-species peaks at S1/CTAB-GO compared with the other two samples. This is due to the existence of the interactions between GO and CTAB. GO contains O-based functional groups such as –OH and –COOH, which can provide functional groups with negative charges bonded to the GO flakes, and further bonded with CTA^+.

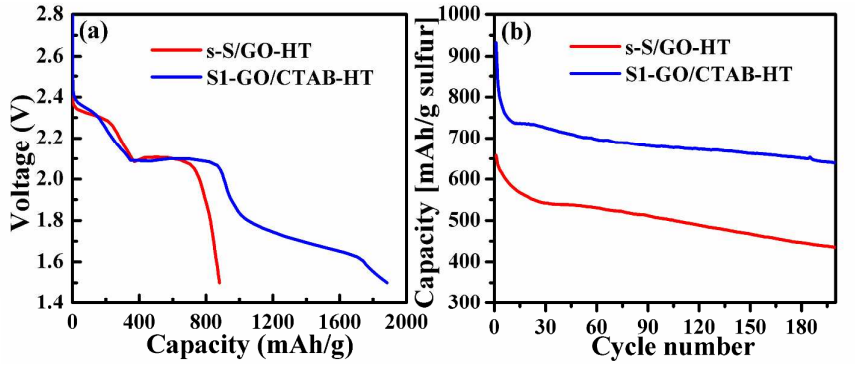

Figure 5: (a) Galvanostatic discharge profiles and (b) cell performances of samples s-S/GO-HT and S1-GO/CTAB-HT.

Therefore if the GO suspension was mixed with CTAB solution, some of the CTA^+ cations will be bonded to GO, leading to a decrease of the amount of the CTA^+ cations that can bond to S_x^{2-} when mixed with Na_2S_x solution.

Overall, these observations further prove that the introduction of CTAB can significantly influence the final products of the reaction, while the application of GO can influence the morphological structure of the cathode active material. The presence of the interactions among the sulfur layer, CTAB and GO can benefit the immobilization of sulfur. Moreover, the interaction between S_x^{2-} and CTAB may help trap the lithium polysulfides during a charge-discharge process. Both effects can suppress the diffusion of the lithium polysulfides into the electrolyte during the

charge/discharge process; thereby suppressing the polysulfide shuttle, which is a widely-observed problem for the sulfur electrode.

3.3. Cell Performance Enhancement With the Introduction of CTAB

As discussed above, the introduction of CTAB can change the chemical structure of the cathode material, as demonstrated by both the SEM and the S K-edge XAS data. To gain deeper insight to the effect of the CTAB on the cell performance, we used the heat-treated S-GO and CTAB-S-GO (s-S/GO-HT and S1-GO/CTAB-HT) as cathode materials in Li/S cells. We took these two samples as examples because they differ only in the presence of CTAB, so a comparison of these two samples can give information on the effect of this additive. Figure 5 (a) shows the first cycle discharge voltage profiles of the electrodes at the rate of 0.2 C (1C=1675 mAh/gS). As can be seen, the S-GO and CTAB-S-GO nanocomposites deliver initial discharge capacities of about 826 and 1894 mAh/g at 0.2 C, respectively. The cathode based on sample S1-GO/CTAB-HT showed a significantly higher initial capacity over that of sample s-S/GO-HT. Moreover, an additional plateau can be observed in the region of 1.8-1.6 V for the sample S1-GO/CTAB-HT, which indicates that CTAB acts as a protective layer and strongly bonds with S. Although the cells are not fully optimized, we can see that the CTAB-S-GO based Li/S cell shows significant improvement of capacity and capacity decay rate compared with the S-GO based cell during the first 200 cycles, as shown in Figure 5 (b). This proves that the introduction of CTAB can benefit the Li/S cell performance due to the appearance of C-S bonds and the existence of interactions between CTAB and S_x^{2-} in the charged/discharge process.

4. CONCLUSION

We applied S K-edge XAS to study the S species evolution during the synthesis of the CTAB-S-GO nanocomposites used as cathode materials in Li/S cell. This study revealed the interactions among CTAB, GO and S/S_x^{2-}. The results indicate that CTAB interacts with S_x^{2-} and remains in the cathode material when precipitated from solution and this kind of bonding can be converted to chemical C-S bonds after heat treatment at 155°C. GO can not only bond with CTAB but also act as a nucleation center for S precipitation. Thus the interaction of CTAB with GO, C-S bonds between

CTAB and S, and the attached S layer on GO provides a tight tri-layer structure which can immobilize the S on the GO sheet and enhance the cell performance. This work demonstrates the importance of the S precursor components, CTAB and GO addition procedures in the synthesis, which can be readily used to optimize the active material. Although our work has proved that the introduction of CTAB to the S-GO system can significantly improve the cell performance, there are still some more parameters that can be optimized. We hope the information from the XAS studies can offer a new strategy to explore and develop better S nanocomposite-based cathodes for advanced Li/S cells that can be used for scaled-up applications.

AUTHOR INFORMATION

Corresponding authors:

*jfzhu@ustc.edu.cn, jguo@lbl.gov, ejcairns@lbl.gov

Notes

The authors declare no competing financial interests.

ACKNOWLEDGEMENTS

We thank Wayne Stolte, Josep Roque-Rosell, Sirine Fakra and Richard Celestre for the technical support at the ALS beamlines. J.Z. gratefully acknowledges the financial support from the National Basic Research Program of China (2013CB834605), the National Natural Science Foundation of China (U1232102, 21173200, 21473178), and Scientific Research and Users with Potential Grants of Hefei Science Center of CAS (2015SRG-HSC031, 2015HSC-UP022). The Advanced Light Source is supported by the Director, Office of Science, Office of Basic Energy Sciences, of the U.S. Department of Energy under Contract No. DE-AC02-05CH11231. Y.Y thanks the support of ALS Doctoral Fellowship.

ASSOCIATED CONTENT

Supporting Information:

Supporting Information Available: Detailed sample preparation, cell assembly and testing process. S K-edge XAS characterization of intermediate species of s-S/CTAB (Figure S1), mixture of elemental S and CTAB dissolved in formic acid (Figure S2) and samples of S1-GO/CTAB, S1/CTAB-GO and s-S/CTAB (Figure S3). The supporting information is available free of charge on the ACS Publication Website http://pubs.acs.org.

REFERENCES:

1. Song, M.-K.; Cairns, E. J.; Zhang, Y., Lithium/Sulfur Batteries with High Specific Energy: Old Challenges and New Opportunities. *Nanoscale* **2013**, *5*, 2186-2204.

2. Li, W.; Zheng, G.; Yang, Y.; Seh, Z. W.; Liu, N.; Cui, Y., High-Performance Hollow Sulfur Nanostructured Battery Cathode through a Scalable, Room Temperature, One-Step, Bottom-up Approach. *Proc. Natl. Acad. Sci. USA* **2013**, *110*, 7148-7153.

3. Song, M.-K.; Zhang, Y.; Cairns, E. J., A Long-Life, High-Rate Lithium/Sulfur Cell: A Multifaceted Approach to Enhancing Cell Performance. *Nano Lett.* **2013**, *13*, 5891-5899.

4. Roy, P.; Srivastava, S. K., Nanostructured Anode Materials for Lithium Ion Batteries. *J. Mater. Chem. A* **2015**, *3*, 2454-2484.

5. Bruce, P. G.; Freunberger, S. A.; Hardwick, L. J.; Tarascon, J.-M., Li-O_2 and Li-S Batteries with High Energy Storage. *Nat. Mater.* **2012**, *11*, 19-29.

6. Ji, X.; Nazar, L. F., Advances in Li-S Batteries. *J. Mater. Chem.* **2010**, *20*, 9821-9826.

7. Manthiram, A.; Fu, Y.; Su, Y.-S., Challenges and Prospects of Lithium–Sulfur Batteries. *Acc. Chem. Res.* **2013**, *46*, 1125-1134.

8. Qiu, Y., Li, W., Zhao, W., Li, G., Hou, Y., Liu, M., Zhou, L., Ye, F., Li, H., Wei, Z., et al., High-Rate, Ultralong Cycle-Life Lithium/Sulfur Batteries Enabled by Nitrogen-Doped Graphene. *Nano Lett.* **2014**, *14*, 4821-4827.

9. Manthiram, A.; Fu, Y.; Chung, S.-H.; Zu, C.; Su, Y.-S., Rechargeable Lithium–Sulfur Batteries. *Chem. Rev.* **2014**, *114*, 11751-11787.

10. Mikhaylik, Y. V.; Akridge, J. R., Polysulfide Shuttle Study in the Li/S Battery System. *J. Electrochem. Soc.* **2004**, *151*, A1969-A1976.

11. Zhang, Q.; Wang, Y.; Seh, Z. W.; Fu, Z.; Zhang, R.; Cui, Y., Understanding the Anchoring Effect of Two-Dimensional Layered Materials for Lithium-Sulfur Batteries. *Nano Lett.* **2015**, *15*, 3780–3786.

12. Elazari, R.; Salitra, G.; Garsuch, A.; Panchenko, A.; Aurbach, D., Sulfur-Impregnated Activated Carbon Fiber Cloth as a Binder-Free Cathode for Rechargeable Li-S Batteries. *Adv. Mater.* **2011**, *23*, 5641-5644.

13. Ji, L.; Rao, M.; Zheng, H.; Zhang, L.; Li, Y.; Duan, W.; Guo, J.; Cairns, E. J.; Zhang, Y., Graphene Oxide as a Sulfur Immobilizer in High Performance Lithium/Sulfur Cells. *J. Am. Chem.*

Soc. **2011**, *133*, 18522-18525.

14. Jayaprakash, N.; Shen, J.; Moganty, S. S.; Corona, A.; Archer, L. A., Porous Hollow Carbon@Sulfur Composites for High-Power Lithium–Sulfur Batteries. *Angew. Chem. Int. Ed.* **2011**, *50*, 5904-5908.

15. Ji, X.; Lee, K. T.; Nazar, L. F., A Highly Ordered Nanostructured Carbon-Sulphur Cathode for Lithium-Sulphur Batteries. *Nat. Mater.* **2009**, *8*, 500-506.

16. Wang, C.; Wang, X.; Yang, Y.; Kushima, A.; Chen, J.; Huang, Y.; Li, J., Slurryless Li_2S/Reduced Graphene Oxide Cathode Paper for High-Performance Lithium Sulfur Battery. *Nano Lett.* **2015**, *15*, 1796-1802.

17. Wu, F.; Lee, J. T.; Magasinski, A.; Kim, H.; Yushin, G., Solution-Based Processing of Graphene–Li_2S Composite Cathodes for Lithium-Ion and Lithium–Sulfur Batteries. *Part. Part. Syst, Char.* **2014**, *31*, 639-644.

18. Feng, X.; Song, M.-K.; Stolte, W. C.; Gardenghi, D.; Zhang, D.; Sun, X.; Zhu, J.; Cairns, E. J.; Guo, J., Understanding the Degradation Mechanism of Rechargeable Lithium/Sulfur Cells: A Comprehensive Study of the Sulfur-Graphene Oxide Cathode after Discharge-Charge Cycling. *Phys. Chem. Chem. Phys.* **2014**, *16*, 16931-16940.

19. Zhang, L.; Ji, L.; Glans, P.-A.; Zhang, Y.; Zhu, J.; Guo, J., Electronic Structure and Chemical Bonding of a Graphene Oxide-Sulfur Nanocomposite for Use in Superior Performance Lithium-Sulfur Cells. *Phys. Chem. Chem. Phys.* **2012**, *14*, 13670-13675.

20. Braun, A.; Wang, H.; Bergmann, U.; Tucker, M. C.; Gu, W.; Cramer, S. P.; Cairns, E. J., Origin of Chemical Shift of Manganese in Lithium Battery Electrode Materials—a Comparison of Hard and Soft X-Ray Techniques. *J. Power Sources* **2002**, *112*, 231-235.

21. Braun, A.; Janousch, M.; Sfeir, J.; Kiviaho, J.; Noponen, M.; Huggins, F. E.; Smith, M. J.; Steinberger-Wilckens, R.; Holtappels, P.; Graule, T., Molecular Speciation of Sulfur in Solid Oxide Fuel Cell Anodes with X-Ray Absorption Spectroscopy. *J. Power Sources* **2008**, *183*, 564-570.

22. Nurk, G.; Huthwelker, T.; Braun, A.; Ludwig, C.; Lust, E.; Struis, R. P. W. J., Redox Dynamics of Sulphur with Ni/Gdc Anode During Sofc Operation at Mid- and Low-Range Temperatures: An Operando S k-Edge Xanes Study. *J. Power Sources* **2013**, *240*, 448-457.

23. Cuisinier, M.; Cabelguen, P.-E.; Evers, S.; He, G.; Kolbeck, M.; Garsuch, A.; Bolin, T.; Balasubramanian, M.; Nazar, L. F., Sulfur Speciation in Li–S Batteries Determined by Operando X-Ray Absorption Spectroscopy. *J. Phys. Chem. Lett.* **2013**, *4*, 3227-3232.

24. Fong, R.; Dahn, J. R.; Jones, C. H. W., Electrochemistry of Pyrite‐Based Cathodes for Ambient Temperature Lithium Batteries. *J. Electrochem. Soc.* **1989**, *136*, 3206-3210.

25. Jalilehvand, F., Sulfur: Not a "Silent" Element Any More. *Chem. Soc. Rev.* **2006**, *35*, 1256-1268.

26. Ye, Y.; Kawase, A.; Song, M.-K.; Feng, B.; Liu, Y.-S.; Marcus, M.; Feng, J.; Cairns, E.; Guo, J.; Zhu, J., X-Ray Absorption Spectroscopy Characterization of a Li/S Cell. *Nanomaterials* **2016**, *6*, 14.

27. Ota, H.; Akai, T.; Namita, H.; Yamaguchi, S.; Nomura, M., Xafs and Tof–Sims Analysis of Sei Layers on Electrodes. *J. Power Sources* **2003**, *119–121*, 567-571.

28. Vairavamurthy, A., Using X-Ray Absorption to Probe Sulfur Oxidation States in Complex Molecules. *Spectrochim. Acta A* **1998**, *54*, 2009-2017.

29. Pascal, T. A., Wujcik, K. H., Velasco-Velez, J., Wu, C., Teran, A. A., Kapilashrami, M., Cabana, J., Guo, J., Salmeron, M., Balsara, N., et al., X-Ray Absorption Spectra of Dissolved Polysulfides in Lithium–Sulfur Batteries from First-Principles. *J. Phys. Chem. Lett.* **2014**, *5*, 1547-1551.

30. Huang, L.; Chen, X.; Li, Q., Synthesis of Microporous Molecular Sieves by Surfactant Decomposition. *J. Mater. Chem.* **2001**, *11*, 610-615.

TOC GRAPHICS